Dye Adsorption of Biochar

Subjects: Environmental Sciences

Contributor: Lalit Goswami, Anamika Kushwaha, Saroj Raj Kafle, Beom-Soo Kim

Biochar (BC) is a highly stable carbonaceous material that is aromatized and amorphous in nature. It is usually formed after thermochemical conversion of organic matter and wastes at temperatures of 350–750 °C under limited oxygen conditions. It is being studied to a great degree because of its potential for carbon sequestration, soil improvement, climate change mitigation, catalysis, wastewater treatment, energy storage, and waste management.

Keywords: post-processing modification ; surface-engineered biochar ; dye removal

1. Production of Biochar

Various methods have been employed for BC production, such as combustion, torrefaction, gasification, and pyrolysis (slow and fast types) [1]. Each method results in a different char yield and carbon level. These processes differ based on temperature, char yield, heating rate, feedstock residence time, and carbon content and yield. Earlier, combustion was used to produce charcoal from woody biomass; however, it resulted in low yields and extreme air pollution. With time, the advancement in technology (endothermic and exothermic processes) allows the maximum energy extraction from organic matter. Combustion and gasification generate heat and gas, respectively, by thermally decomposing organic matter in an oxic environment [2]. However, these processes are less effective and satisfactory in decreasing emissions while meeting energy requirements. On the other hand, pyrolysis is the most common, oldest, and the most effective process for meeting energy requirements and reducing emissions. **Figure 1** depicts the mechanism of BC formation from cellulose, hemicellulose, and lignin [3]. Pyrolysis leads to the production of BC (solid), bio-oil (liquid), and syngas (gas). The generated by-products can also be utilized as energy substances to meet the energy crisis.

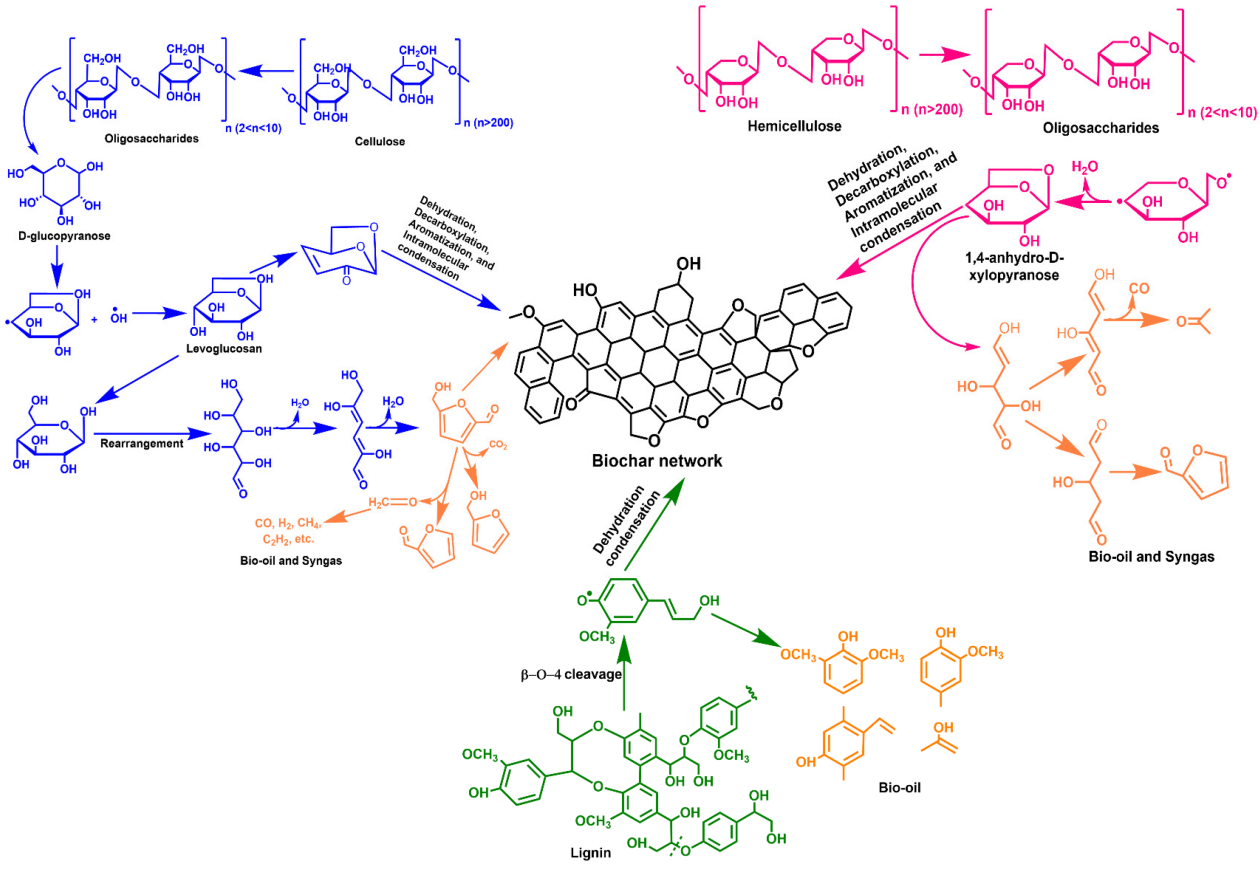

Figure 1. Mechanism of biochar formation from cellulose, hemicellulose, and lignin.

Here, pyrolysis can be classified into slow, intermediate, and fast pyrolysis in accordance with the heating rate, temperature, pressure, and residence time [4]. For high yield of BC, slow pyrolysis should meet heating rate of 0.1–1 °C min^{-1}, whereas fast pyrolysis and high temperature can result in generation of more liquid and syngas. In addition, the mass fraction range of pyrolysis solid increases with increasing temperature. In case of intermediate pyrolysis where the conditions are between slow and fast pyrolysis, there is a balance yield of BC and bio-oil yield, but it is rarely approved from a BC production perspective [5][6]. Further, the properties of BC depend on numerous factors and parameters such as pyrolysis temperature and type of feedstock.

Some conceivable approaches for more efficient BC production are proposed as follows: (i) improving energy efficiency via utilization of batch reactors through continuous feeding pyrolyzers; (ii) enhancing energy efficiency and BC yield using exothermic operation; (iii) tuning the BC properties (texture feature and surface chemistry) by adjusting the operating conditions; (iv) improving process economics and reducing pollutant emissions; (v) exploring new biomass-based feedstocks [7].

2. Characteristics of Biochar

2.1. Physical Properties

The physical properties of BC are directly dependent on the biomass feedstock and pyrolysis conditions, including biomass pre-treatment and handling. In particular, the attrition, crack formation, and microstructural rearrangement generated under different pyrolysis conditions change the native structure of the biomass feedstock to varying degrees [7]. As the pyrolysis process progresses, the biomass feedstock is reduced, converting macropores into mesopores and micropores. The ideal BC physical structure can be enhanced by increasing the pyrolysis temperatures to the point where deformation occurs [8]. Thermal decomposition of organic materials begins at >120 °C. More specifically, hemicellulose, cellulose, and lignin decompose at 200–260 °C, 240–350 °C, and 280–500 °C, respectively.

2.1.1. Nano and Macroporosity

The pore size distribution is one of the most important physical properties. Macropores (>50 nm), mesopores (2–50 nm), and micropores (<2 nm) constitute the total pore volume of BC. Here, micropores are the prime contributors to the BC surface area and are also responsible for efficient adsorbents, whereas mesopores play a noteworthy role in the liquid–solid adsorption process [7][9]. Further, micropores are amended via prolonging pyrolysis at higher temperatures which simultaneously release the volatile content of the feedstock along with the creation of numerous pores. Slow pyrolysis enhances the porosity of BC via slow decomposition of lignin content. The surface area of BC increases quickly when the pyrolysis temperature exceeds >400 °C, owing to thermal condensation of the biomass feedstock and micropore formation [8]. Biomass possessing aromatic lignin cores, aliphatic alkyl, and ester groups produces a higher surface area when pyrolyzed at higher temperatures.

2.1.2. Particle Size Distribution

BC particle size is determined by biomass rigidity against shrinkage and slow destruction during the pyrolysis process. Usually, the BC particle sizes are smaller compared to the un-pyrolyzed biomass. However, agglomeration may occur during pyrolysis, resulting in BC with a larger particle size [7]. Post-mechanical stresses may also occur, crumbling BC more susceptible than the original biomass. Slow pyrolysis (5–30 °C/min) results in a smaller size of BC. BC particle size has an inverse correlation with reaction temperature. For instance, an increase in reaction temperature (450 °C to 700 °C) results in the formation of smaller size particles [4]. This could be due to the augmented susceptibility to attrition because of the lower biomass/BC tensile strength [10].

2.1.3. Density

Apparent/bulk/solid density can be evaluated relating to determining the physical properties of BC. Usually, there is an antagonistic relationship between bulk density and solid density. In general, the solid density of BC is higher than that of the original biomass as a result of the release of volatile and condensable compounds and the formation of graphitic crystallites [7][10]. In contrast, BC has a lower bulk density compared to wood precursor owing to biomass drying and carbonization.

2.1.4. Mechanical Strength

This property correlates directly with density and inversely with porosity. Few studies have reported the evaluation of mechanical strength of BC [11]. In comparison to the virgin wood, monolithic carbonized wood BC has lower stiffness (37%) and higher strength (28%). Here, both the reduced modulus and hardness of pyrolyzed wood BC incessantly

increases with increasing temperature (between 700 and 2000 °C) [12]. A negative effect on these properties follows with a further increase in the pyrolysis temperature. In addition, compared to harder native woods (low ash and high lignin content), fruit stones/pits and nutshells are more appreciated for BC production depicting admirable mechanical properties [7]. Further, it was found that the pyrolytic temperature is more dominant than the residence time in determining the mechanical properties of BC.

2.2. Chemical Properties

BC properties depend on the biomass type and pyrolysis temperature. In fact, data on synthesis techniques can be used to predict the properties and functions of BC [13]. In general, with a surge in pyrolysis temperature, BC yield declines exponentially while BC alkalinity (pH) displays a linear rise [7][13]. The increase in pH can be ascribed to thermal decomposition of hydroxyl groups and other weak bonds within the BC structure at high temperatures. In comparison, due to the removal of acidic functional groups, the cation exchange capacity of BC is inversely proportional to the pyrolysis temperature [7][13]. BC derived from biosolids display the highest cation exchange capacity due to the presence of minerals (P, Mg, Ca, Na, and K) in the biosolids, which encourage the generation of oxygen-containing functional groups on the surface of BC [14]. Unlike ash, the volatile matter content of BC decreases linearly with increasing pyrolysis temperature. Ash formation is due to inorganic minerals remaining following the decomposition of H, O, and C of biomass [13]. The destruction of hydroxyl, azanide, and other weakly bonded groups results in the reduction of these elements with increasing temperature. However, the C content gradually declines, resulting in a higher C content in the BC at the enhanced pyrolysis temperatures [13].

2.3. Microchemical Characteristics

BC microchemical properties can influence its superficial sorption characteristics. The microchemical properties vary significantly depending on the nature and composition of solid phase, entrapped oils and their arrangement, and indicate the electrochemical properties and functional groups on the BC surface [7][15]. Dried biomass pyrolysis is activated by hemolytic cleavage of covalent bonds to release free radicals and structural O [15]. In the initial phases of pyrolysis, free radicals are generated from low atmospheric O_2 levels [7][14][15]. This process proceeds with the formation of carboxyl and carbonyl groups, followed by their cleavage into CO_2 and CO. Finally, BC residues are produced from free radical fragments that recombine with the substrate in various ways [15].

2.4. Organo-Chemical Characteristics

In general, the H-to-C ratio declines from ~1.5 to ≤0.5 in lignocellulosic biomass with pyrolysis temperatures of >400 °C. This reduction in the H-to-C ratio could be due to changes in the elemental (N, O, H, and C) content during thermal decomposition of the biomass. O-to-C and H-to-C ratios (displaying the degree of aromaticity and maturation) in BC decrease at higher reaction temperatures [4][7]. Burnt peat displayed an H-to-C ratio of 1.3 when the maximum C content was either associated through a hydroxyl group or directly bonded to a proton. If the H-to-C ratio drops to 0.4–0.6, it indicates that every second to third C is associated with a proton [7].

3. Factors Influencing Biochar Sorption Efficiency

BC is a carbonaceous material derived via biomass thermal conversion (pyrolysis, gasification, hydrothermal carbonization, and torrefaction) under oxygen-limited conditions [16]. Typically, cellulose (40–60%), hemicellulose (20–40%), and lignin (10–25%) are included within biomass [17]. Biomass structural building blocks undergo a sequence of reactions during thermal decomposition, such as dehydration, de-polymerization, rearrangement, re-polymerization, condensation, and carbonization at various temperatures, producing BC, bio-oil, and syngas [18]. Based on the feedstock, the desired product and its application vary. Biomass characteristics include elemental composition, size, and ash mineral content, whereas thermal conditions include temperature, heating rate, pressure, and residence time [4][19]. Several parameters affect BC performance during adsorption. BC physisorption isotherm characteristics govern properties such as morphological structure and reactivity depending on pyrolytic conditions.

3.1. Temperature

Reaction temperature plays a vital role in the process and reaction rate. Huang et al. [20] suggested that the adsorption is chemical rather than physical when the equilibrium temperature does not significantly affect the adsorption process. Based on the pore size, adsorbent materials of various sizes are grouped into micropores, mesopores, and macropores, which are highly dependent upon the production conditions of BC. BC produced by pyrolysis at high temperatures

contains high micropore volumes ranging from 50% to 70% of the total pores. Adsorption of contaminants by BC is an endothermic process and the adsorption capacity increases with increasing temperature.

An experimental study was conducted by Tan et al. [21] on Cu (II) adsorption and textile dye adsorption into food waste BC, and thermodynamics parameters were calculated. In both cases, the heat of reaction was positive and Gibbs's free energy was negative. According to Ambaye et al. [22], as the reaction temperature increases, the BC surface area increases as the amount of oxygen-containing functional groups on the surface decreases. Wu et al. [23] used litchi peel biomass and increased the activated temperature from 650 °C to 850 °C, which ultimately increased the surface area from 531 m^2 g^{-1} to 1006 m^2 g^{-1} and the pore volume from 0.328 cm^{-1} g^{-1} to 0.588 cm^{-1} g^{-1}.

One experimental setup was carried out by Qambrani et al. [24] to perceive the effect of temperature on BC yield and quality. The yield, total nitrogen and organic carbon content, and cation exchange capacity values were found to decrease with increasing pyrolysis temperature. Therefore, low temperatures are highly recommended for BC production from poultry litter. This condition applies analogously to the condition for BC obtained from vegetative materials.

3.2. Solution pH

Solution pH plays a vital role in controlling the surface charge of the adsorbent and the degree of ionization of adsorbate [25]. At high pH, a negative charge exists on the surface with deprotonation of the phenolic and carboxylic groups. At low pH, basic functional groups become protonated and positively charged, promoting adsorption of anions. Adsorption by BC is known to be a function of pH, medium, and deprotonation of functional groups [26]. The pH at the zero-point change is the point at which the net charge on the surface of any adsorbent in solution becomes neutral. At this point, pH highly affects the adsorption efficiency of the BC active surface by providing active functional groups for a charged solution. Therefore, increasing the pH of a solution containing BC leads to a negative potential by increasing the negative charge on the BC surface [27].

Qiu et al. [28] reported that the positive charge on activated carbon at pH 3.0 was higher than at pH 6.5. In contrast, the negative charge on BC was more negative at pH 6.5. Therefore, BC was more efficient than activated carbon at adsorbing dyes from solution. Similarly, the effect of pH on methylene blue dye adsorption was studied at various pH (2–10) [29]. As the pH increases, the number of positively charged sites decreases, increasing methylene blue adsorption. Although the high adsorption of the methylene blue is favorable in alkaline solution, the adsorption did not change when the pH of the solution increased. They observed a maximum dye adsorption (69.07%) at pH 4 [29]. Lin et al. [30] tested the microalgae derivative BC to remove dye and found that the higher the pH of the aqueous solution, the greater the adsorption capacity of positively charged dyes with surface electrostatic attraction due to the negative potential effects. Similarly, Huang et al. [31] studied the removal of organic dye using BC derived from *Spirulina platensis* algae biomass residue. The maximum adsorption capacity was obtained at the alkaline pH with an adsorbent dosage of 2000 mg/L and an initial dye concentration of 90 mg/L.

3.3. Adsorbent Dosage

The adsorbent dosage greatly influences the sorbent-sorbate equilibrium in the adsorption system. Due to the availability of more sorption sites, the removal efficiency of organic and inorganic pollutants increases with increasing adsorbent dosage. When the dosage rate is in excess, the adsorption capacity of BC decreases [26]. The reduction in adsorption may be attributed to the overlap of adsorption sites which ultimately shield the pores [26]. Moreover, at a lower dosage of adsorbent at a given initial dye concentration, the ratio of dye to adsorbent molecules increases, leading to an increase in specific uptake. In contrast, at a higher dosage of adsorbent, the availability of dye ions is insufficient for adsorption to the sites [31].

The effect of adsorbent dosage of BC derived from eucalyptus bark to remove methylene blue dye from aqueous solution was studied [31]. They observed that the dye adsorption decreased from 56.8 to 25.5 (mg/g) as the adsorbent dosage was increased from 0.01 to 0.03 g. According to Zhang et al. [32], Congo red dye removal (82.2–83.6%) increased as the adsorbent dosage was increased from 0.2 to 1 g/100 mL. Green BC composite was used for methylene blue removal with adsorbent doses up to 2 g/L. It was found that the adsorption performance decreases with increasing dosage, reducing the number of methylene blue molecules per unit adsorbent [32].

3.4. Initial Dye Concentration

For an efficient and effective adsorption process, the initial concentration of adsorbate plays a vital role. As the initial dye concentration increases, the percentage removal of dye increases. The initial dye concentration provides the driving force

to overcome the mass transfer resistance of dye between the aqueous and solid phases [29]. According to Chowdhury et al. [33], at high concentrations, all dye molecules in solution do not interact with the binding sites of the adsorbent because the adsorbent has a limited number of active binding sites that saturate at a certain concentration. Experimental work carried out by Dawood et al. [34] found that the percentage of methylene blue removal decreased from 80.5% to 36.8% as the initial concentration (10–100 mg/L) of the methylene blue dye solution increased. Another experimental work was also carried out in which the percentage removal of methylene blue dye drastically reduced from 85.93% to 41.40% with increasing initial dye concentration (20 to 50 mg/L) [35].

3.5. Heating Rate

The heating rate is also one of the major factors affecting BC properties. According to Xu and Chen [36], heating rates of <20 °C s^{-1} for BC production from pine sawdust permitted the natural porosity of sawdust to be shifted to BC without significant structural variations. In contrast, devolatilization occurred at a heating rate of 500 °C s^{-1}, resulting in deformation of the sawdust cell structure. Finally, lower pyrolysis temperature and lower heating rate along with high residence time led to BC formation. Li et al. [37] produced BC from lignin (heating rate of 10 °C min^{-1}) and the abundance of -OH started to decrease from 350 °C. They concluded that a lower heating rate with long residence time increased the thermal stability of the -OH functional groups on the BC surface. BC carbon content increased from 75.39% to 88.35%, 75.15% to 88.28%, and 77.13% to 89.70% at various heating rates 5, 10, and 15 °C min^{-1}, respectively. Li et al. [37] concluded that the smaller particle size leads to a complete pyrolysis process, and the hydrogen, sulfur, and oxygen content decreases with increasing temperature. With an upsurge in temperature, the H/C and O/C atoms gradually decrease and BC becomes more carbonaceous and aromatic.

3.6. Particle Size

The rate of heat and mass transfer of particles and the degree of subordinate reactions are significantly influenced by the particle size of the biomass. The particle size depends on the process being carried out and the feedstock materials. Larger particle sizes (>1.8 mm) have greater temperature gradients and thus provide higher BC in comparison with smaller particle sizes [24]. An experiment was conducted with various particle sizes of wood, and it was observed that maximum BC yield (28%) was attained with particle sizes 0.224–0.425 nm at 500 °C and 223.15 °C min^{-1} heating rate in an inert environment [38]. Mechanical properties such as mechanical strength, yield stress, and BC density are highly dependent on biomass particle size. As a result of examining the effect of particle size on wood biomass, it was found that wood BC produced from smaller particle sizes showed higher yield stress and density compared to larger ones [39]. The smaller particle size is appropriate for fast pyrolysis due to the uniform and effective heat transfer facilitating the release of volatiles.

3.7. Feedstock Composition

Feedstock selections also greatly impact BC properties and elemental composition. It affects various physical properties of BC, such as pH, pore structure, surface area, adsorption efficiency, and other chemical properties [7]. Compared to cellulose, hemicellulose, lignin, and some organic compounds, a feedstock consisting of animal manure results in higher BC nutrients. As the temperature increases, the volatile compounds in the biomass decrease along with a decrease in the quantity of surface functional groups, but the surface area and ash content of BC increase [4][9]. Feedstock materials are oxygen-rich and hydrogen-deprived, for example, sugars are non-graphitizing and create robust cross-linked arrangements that immobilize the structure and tie the crystallites into a stiff mass. The various carbon and nitrogen contents in char produced from plant-derived biomass were found to be increased relative to biomass. However, the use of mineral-rich feedstock (manure) may reduce it [40].

4. Mechanisms of Dye Adsorption

The enhanced performance of BC (without activation) can be due to oxygen containing surface functional groups and other inorganic components that play a significant role in dye adsorption instead of only surface area and porosity. BC inorganic elements upsurge the hydrophilicity towards dyes and act as catalysts during the adsorption process [41]. However, BC activation, surface area, and surface alkalinity can also influence adsorption capacity. **Figure 2** represents the adsorption process and mechanism for dye removal from wastewater. Specific adsorption mechanisms include (i) physical adsorption, (ii) ion exchange; (iii) electrostatic interactions; (iv) precipitation; and (v) surface complexation [7][8]. However, the pollutant removal process always works in conjunction with numerous mechanisms.

4.1. Physical Adsorption

Dye adsorption onto the BC surface primarily occurs via physical interactions such as pore filling, π stacking, and H-bonding. However, BC surface area, porosity, and aromaticity influence the physical adsorption. The enhanced surface area and pore volume favor the diffusion of contaminants [42]. The aromatic structure of BC is promising for forming π-stacking and H-bond interactions with pollutants [43]. The pore filling, π–π interactions, and H bonding between BC and dye can be improved via post-modification of BC. For example, pore filling is an illustrative of physical adsorption and can be accredited to a widespread distribution of pores via BC [44]. Hydroxyl and amine groups can be an advantage for π–π interactions due to electron-deficient functional groups on the surface of cationic dyes [45]. For instance, cationic dyes H-bonding of O and/or N center generated free hydroxyl groups on the surface of sulfur-doped tapioca peel waste BC [46], whereas fly ash and agricultural waste-derived BC alkali-fusing with O-containing surface groups resulted in H-bonding [47]. The generation of H-bonds between acid orange 7 dye and the adsorbent accounts for the adsorption process [48]. Siddiqui et al. reported the H-bonds between methylene blue and MnO_2/BC occurs due to the interaction between the -OH groups present in MnO_2/BC and the acceptor present in the methylene blue molecules [49]. Likewise, π–π interactions/π-effects/π-interactions (non-covalent) involve the π system, where positively charged molecules interact with negatively charged surfaces, similar to electrostatic interactions [7].

4.2. Ion Exchange

Dye adsorption on the BC surface occurs via exchange of metal ions/mineral elements or replacement of BC functional groups [42]. Furthermore, the ion exchange mechanism involves ion exchange between a liquid (dye solution) and a solid phase (adsorbent). Pirbazari et al. suggested that two principal mechanisms are involved in the removal of methylene blue dye on NaOH-treated wheat straw impregnated with Fe_3O_4, namely, surface complex formation and ion exchange between the dye molecules and adsorption surfaces [50]. According to Zheng et al., the adsorption of anionic dyes such as Congo red and methyl orange on graphene oxide-NiFe layered double hydroxide is achieved by electrostatic attraction and ion exchange phenomena [51].

4.3. Electrostatic Attraction

Synthetic dyes are categorized into cationic and anionic dyes. Malachite green, methylene blue, and rhodamine B are examples of cationic dyes [52], and tartrazine, sunset yellow, Congo red, and orange G are examples of anionic dyes [53]. Knowledge of dye classification aid in choosing the accurate adsorbent as a positively charged adsorbent is effective in removing negatively charged dyes due to electrostatic interactions [53]. An electrostatic attraction occurs between the dye and BC surface when the surface charges are opposite [54]. Electrostatic interaction is one of the prime adsorption mechanisms for the adsorption of synthetic dyes on BC and can influence the adsorption rate. For instance, BC derived from litchi peel was assessed for adsorption of anionic and cationic dyes. The adsorption capacity was 404.4 and 2468 mg g^{-1}, respectively [23]. However, other adsorption mechanisms were also involved in the adsorption, and since the dye and BC both have opposite charges, the dye adsorption significantly occurred via electrostatic interactions [23]. Several BCs were designed for cationic and anionic dyes that fit either pseudo-second order or Elovich kinetic models, where both are indicative of electrostatic interactions and chemisorption. Shen and Gondal reported that electrostatic and intermolecular interactions govern the adsorption of rhodamine dye on adsorbent surfaces [55].

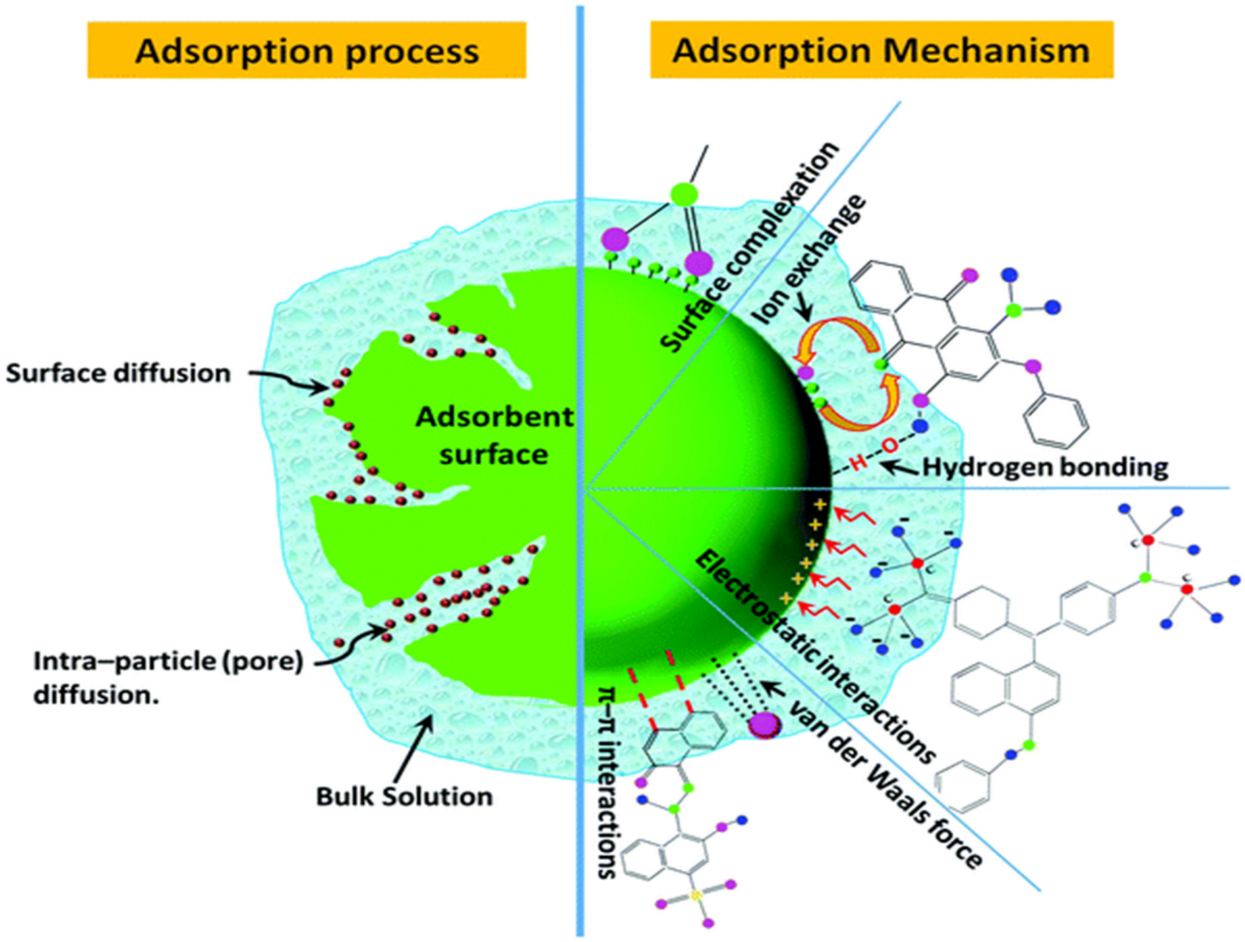

Figure 2. Adsorption process and mechanism for dye removal from wastewater [56].

References

1. Al-Rumaihi, A.; Shahbaz, M.; Mckay, G.; Mackey, H.; Al-Ansari, T. A review of pyrolysis technologies and feedstock: A bl ending approach for plastic and biomass towards optimum biochar yield. Renew. Sustain. Energy Rev. 2022, 167, 1127 15.
2. Zaman, C.Z.; Pal, K.; Yehye, W.A.; Sagadevan, S.; Shah, S.T.; Adebisi, G.A.; Johan, R.B. Pyrolysis: A Sustainable Way to Generate Energy from Waste; IntechOpen: Rijeka, Croatia, 2017; Volume 1, p. 316806.
3. Liu, W.J.; Jiang, H.; Yu, H.Q. Development of biochar-based functional materials: Toward a sustainable platform carbon material. Chem. Rev. 2015, 115, 12251–12285.
4. Goswami, S.; Kushwaha, A.; Goswami, L.; Gupta, N.R.; Kumar, V.; Bhan, U.; Tripathi, K.M. Nanobiochar-a green cataly st for wastewater remediation. In Bio-Based Nanomaterials; Elsevier: Amsterdam, The Netherlands, 2022; pp. 109–13 2.
5. Zeghioud, H.; Fryda, L.; Djelal, H.; Assadi, A.; Kane, A. A comprehensive review of biochar in removal of organic polluta nts from wastewater: Characterization, toxicity, activation/functionalization and influencing treatment factors. J. Water P rocess Eng. 2022, 47, 102801.
6. Tripathi, M.; Sahu, J.N.; Ganesan, P. Effect of process parameters on production of biochar from biomass waste throug h pyrolysis: A review. Renew. Sustain. Energy Rev. 2016, 55, 467–481.
7. Yaashikaa, P.R.; Kumar, P.S.; Varjani, S.; Saravanan, A. A critical review on the biochar production techniques, charact erization, stability and applications for circular bioeconomy. Biotechnol. Rep. 2020, 28, e00570.
8. Liu, Y.; Chen, Y.; Li, Y.; Chen, L.; Jiang, H.; Li, H.; Hou, S. Fabrication, application, and mechanism of metal and hetero atom co-doped biochar composites (MHBCs) for the removal of contaminants in water: A review. J. Hazard. Mater. 202 2, 431, 128584.
9. Goswami, L.; Pakshirajan, K.; Pugazhenthi, G. Biological treatment of biomass gasification wastewater using hydrocarb onoclastic bacterium Rhodococcus opacus in an up-flow packed bed bioreactor with a novel waste-derived nano-bioch ar based bio-support material. J. Clean. Prod. 2020, 256, 120253.

10. Da Silva Medeiros, D.C.C.; Nzediegwu, C.; Benally, C.; Messele, S.A.; Kwak, J.H.; Naeth, M.A.; El-Din, M.G. Pristine a nd engineered biochar for the removal of contaminants co-existing in several types of industrial wastewaters: A critical r eview. Sci. Total Environ. 2021, 809, 151120.
11. Das, O.; Bhattacharyya, D.; Hui, D.; Lau, K.T. Mechanical and flammability characterisations of biochar/polypropylene b iocomposites. Compos. Part B Eng. 2016, 106, 120–128.
12. Zou, H.; Zhao, J.; He, F.; Zhong, Z.; Huang, J.; Zheng, Y.; Gao, B. Ball milling biochar iron oxide composites for the rem oval of chromium (Cr (VI)) from water: Performance and mechanisms. J. Hazard. Mater. 2021, 413, 125252.
13. Li, S.; Harris, S.; Anandhi, A.; Chen, G. Predicting biochar properties and functions based on feedstock and pyrolysis te mperature: A review and data syntheses. J. Clean. Prod. 2019, 215, 890–902.
14. Agrafioti, E.; Bouras, G.; Kalderis, D.; Diamadopoulos, E. Biochar production by sewage sludge pyrolysis. J. Anal. Appl. Pyrolysis 2013, 101, 72–78.
15. Amonette, J.E.; Joseph, S. Characteristics of biochar: Microchemical properties. In Biochar for Environmental Manage ment; Routledge: London, UK, 2012; pp. 65–84.
16. Mallakpour, S.; Lormahdiabadi, M. Removal of the Anionic Dye Congo Red from an Aqueous Solution Using a Crosslin ked Poly (vinyl alcohol)-ZnO-Vitamin M Nanocomposite Film: A Study of the Recent Concerns about Nonlinear and Lin ear Forms of Isotherms and Kinetics. Langmuir 2022, 38, 4065–4076.
17. Hussain, C.M.; Singh, S.; Goswami, L. Emerging Trends to Approaching Zero Waste; Elsevier: Amsterdam, The Netherl ands, 2021.
18. Goswami, L.; Kushwaha, A.; Singh, A.; Saha, P.; Choi, Y.; Maharana, M.; Kim, B.S. Nano-biochar as a sustainable catal yst for anaerobic digestion: A synergetic closed-loop approach. Catalysts 2022, 12, 186.
19. Vadivel, V.K.; Cikurel, H.; Mamane, H. Removal of Indigo Dye by CaCO3/Ca(OH)2 Composites and Resource Recover y. Ind. Eng. Chem. Res. 2021, 60, 10312–10318.
20. Huang, Q.; Song, S.; Chen, Z.; Hu, B.; Chen, J.; Wang, X. Biochar-based materials and their applications in removal of organic contaminants from wastewater: State-of-the-art review. Biochar 2019, 1, 45–73.
21. Tan, X.; Liu, Y.; Zeng, G.; Wang, X.; Hu, X.; Gu, Y.; Yang, Z. Application of biochar for the removal of pollutants from aq ueous solutions. Chemosphere 2015, 125, 70–85.
22. Ambaye, T.G.; Vaccari, M.; van Hullebusch, E.D.; Amrane, A.; Rtimi, S. Mechanisms and adsorption capacities of bioch ar for the removal of organic and inorganic pollutants from industrial wastewater. Int. J. Environ. Sci. Technol. 2021, 18, 3273–3294.
23. Wu, J.; Yang, J.; Feng, P.; Huang, G.; Xu, C.; Lin, B. High-efficiency removal of dyes from wastewater by fully recycling litchi peel biochar. Chemosphere 2020, 246, 125734.
24. Qambrani, N.A.; Rahman, M.M.; Won, S.; Shim, S.; Ra, C. Biochar properties and eco-friendly applications for climate change mitigation, waste management, and wastewater treatment: A review. Renew. Sustain. Energy Rev. 2017, 79, 25 5–273.
25. Kushwaha, A.; Rani, R.; Kumar, S.; Thomas, T.; David, A.A.; Ahmed, M. A new insight to adsorption and accumulation o f high lead concentration by exopolymer and whole cells of lead-resistant bacterium Acinetobacter junii L. Pb1 isolated f rom coal mine dump. Environ. Sci. Pollut. Res. 2017, 24, 10652–10661.
26. Enaime, G.; Baçaoui, A.; Yaacoubi, A.; Lübken, M. Biochar for wastewater treatment-conversion technologies and appli cations. Appl. Sci. 2020, 10, 3492.
27. Gautam, R.K.; Goswami, M.; Mishra, R.K.; Chaturvedi, P.; Awashthi, M.K.; Singh, R.S.; Pandey, A. Biochar for remediat ion of agrochemicals and synthetic organic dyes from environmental samples: A review. Chemosphere 2021, 272, 1299 17.
28. Qiu, Y.; Zheng, Z.; Zhou, Z.; Sheng, G.D. Effectiveness and mechanisms of dye adsorption on a straw-based biochar. B ioresour. Technol. 2009, 100, 5348–5351.
29. Kaya, N.; Yıldız, Z.; Ceylan, S. Preparation and characterisation of biochar from hazelnut shell and its adsorption prope rties for methylene blue dye. Politek. Derg. 2018, 21, 765–776.
30. Lin, Y.C.; Ho, S.H.; Zhou, Y.; Ren, N.Q. Highly efficient adsorption of dyes by biochar derived from pigments-extracted macroalgae pyrolyzed at different temperature. Bioresour. Technol. 2018, 259, 104–110.
31. Nautiyal, P.; Subramanian, K.A.; Dastidar, M.G. Adsorptive removal of dye using biochar derived from residual algae aft er in-situ transesterification: Alternate use of waste of biodiesel industry. J. Environ. Manag. 2016, 182, 187–197.
32. Zhang, P.; O'Connor, D.; Wang, Y.; Jiang, L.; Xia, T.; Wang, L.; Hou, D. A green biochar/iron oxide composite for methyl ene blue removal. J. Hazard. Mater. 2020, 384, 121286.

33. Chowdhury, S.; Chakraborty, S.; Saha, P. Biosorption of Basic Green 4 from aqueous solution by Ananas comosus (pin eapple) leaf powder. Colloids Surf. B Biointerfaces 2011, 84, 520–527.

34. Dawood, S.; Sen, T.K.; Phan, C. Adsorption removal of Methylene Blue (MB) dye from aqueous solution by bio-char pre pared from Eucalyptus sheathiana bark: Kinetic, equilibrium, mechanism, thermodynamic and process design. Desalin ation Water Treat. 2016, 57, 28964–28980.

35. Biswas, S.; Mohapatra, S.S.; Kumari, U.; Meikap, B.C.; Sen, T.K. Batch and continuous closed circuit semi-fluidized be d operation: Removal of MB dye using sugarcane bagasse biochar and alginate composite adsorbents. J. Environ. Che m. Eng. 2020, 8, 103637.

36. Xu, Y.; Chen, B. Investigation of thermodynamic parameters in the pyrolysis conversion of biomass and manure to bioc hars using thermogravimetric analysis. Bioresour. Technol. 2013, 146, 485–493.

37. Li, C.; Hayashi, J.I.; Sun, Y.; Zhang, L.; Zhang, S.; Wang, S.; Hu, X. Impact of heating rates on the evolution of function groups of the biochar from lignin pyrolysis. J. Anal. Appl. Pyrolysis 2021, 155, 105031.

38. Yorgun, S.; Yıldız, D.; Şimşek, Y.E. Activated carbon from paulownia wood: Yields of chemical activation stages. Energ y Sources Part A Recovery Util. Environ. Eff. 2016, 38, 2035–2042.

39. Harun, N.Y.; Afzal, M.T. Effect of particle size on mechanical properties of pellets made from biomass blends. Procedia Eng. 2016, 148, 93–99.

40. Bourke, J.; Manley-Harris, M.; Fushimi, C.; Dowaki, K.; Nunoura, T.; Antal, M.J. Do all carbonized charcoals have the s ame chemical structure? 2. A model of the chemical structure of carbonized charcoal. Ind. Eng. Chem. Res. 2007, 46, 5 954–5967.

41. Aliasa, N.; Zaini, M.A.A.; Kamaruddin, M.J. Roles of impregnation ratio of K2CO3 and NaOH in chemical activation of p alm kernel shell. J. Appl. Sci. Process Eng. 2017, 4, 195–204.

42. Inyang, M.I.; Gao, B.; Yao, Y.; Xue, Y.; Zimmerman, A.; Mosa, A.; Cao, X. A review of biochar as a low-cost adsorbent fo r aqueous heavy metal removal. Crit. Rev. Environ. Sci. Technol. 2016, 46, 406–433.

43. Ma, J.; Zhou, B.; Zhang, H.; Zhang, W. Fe/S modified sludge-based biochar for tetracycline removal from water. Powde r Technol. 2020, 364, 889–900.

44. Wu, M.; Wang, Y.; Lu, B.; Xiao, B.; Chen, R.; Liu, H. Efficient activation of peroxymonosulfate and degradation of Orang e G in iron phosphide prepared by pickling waste liquor. Chemosphere 2021, 269, 129398.

45. Choudhary, M.; Kumar, R.; Neogi, S. Activated biochar derived from Opuntia ficus-indica for the efficient adsorption of malachite green dye, Cu+2 and Ni+2 from water. J. Hazard. Mater. 2020, 392, 122441.

46. Vigneshwaran, S.; Sirajudheen, P.; Karthikeyan, P.; Meenakshi, S. Fabrication of sulfur-doped biochar derived from tapi oca peel waste with superior adsorption performance for the removal of Malachite green and Rhodamine B dyes. Surf. Interfaces 2021, 23, 100920.

47. Wang, K.; Peng, N.; Sun, J.; Lu, G.; Chen, M.; Deng, F.; Zhong, Y. Synthesis of silica-composited biochars from alkali-f used fly ash and agricultural wastes for enhanced adsorption of methylene blue. Sci. Total Environ. 2020, 729, 139055.

48. Cojocaru, C.; Samoila, P.; Pascariu, P. Chitosan-based magnetic adsorbent for removal of water-soluble anionic dye: Ar tificial neural network modeling and molecular docking insights. Int. J. Biol. Macromol. 2019, 123, 587–599.

49. Siddiqui, S.I.; Manzoor, O.; Mohsin, M.; Chaudhry, S.A. Nigella sativa seed-based nanocomposite-MnO2/BC: An antiba cterial material for photocatalytic degradation, and adsorptive removal of Methylene blue from water. Environ. Res. 201 9, 171, 328–340.

50. Pirbazari, A.E.; Saberikhah, E.; Kozani, S.H. Fe3O4–wheat straw: Preparation, characterization and its application for methylene blue adsorption. Water Resour. Ind. 2014, 7, 23–37.

51. Zheng, Y.; Cheng, B.; You, W.; Yu, J.; Ho, W. 3D hierarchical graphene oxide-NiFe LDH composite with enhanced adso rption affinity to Congo red, methyl orange and Cr (VI) ions. J. Hazard. Mater. 2019, 369, 214–225.

52. Li, H.; Cao, X.; Zhang, C.; Yu, Q.; Zhao, Z.; Niu, X.; Li, Z. Enhanced adsorptive removal of anionic and cationic dyes fro m single or mixed dye solutions using MOF PCN-222. RSC Adv. 2017, 7, 16273–16281.

53. Mahmoud, M.E.; Abdelfattah, A.M.; Tharwat, R.M.; Nabil, G.M. Adsorption of negatively charged food tartrazine and su nset yellow dyes onto positively charged triethylenetetramine biochar: Optimization, kinetics and thermodynamic study. J. Mol. Liq. 2020, 318, 114297.

54. Ho, S.H.; Zhu, S.; Chang, J.S. Recent advances in nanoscale-metal assisted biochar derived from waste biomass used for heavy metals removal. Bioresour. Technol. 2017, 246, 123–134.

55. Shen, K.; Gondal, M.A. Removal of hazardous Rhodamine dye from water by adsorption onto exhausted coffee groun d. J. Saudi Chem. Soc. 2017, 21, S120–S127.

56. Dutta, S.; Gupta, B.; Srivastava, S.K.; Gupta, A.K. Recent advances on the removal of dyes from wastewater using various adsorbents: A critical review. Mater. Adv. 2021, 2, 4497–4531.